PHOTONICS Research

Ultra-high-resolution detection of Pb^{2+} ions using a black phosphorus functionalized microfiber coil resonator

Yu Yin,[1] Shi Li,[1] Shunbin Wang,[1] Shijie Jia,[1] Jing Ren,[1] Gerald Farrell,[2] Elfed Lewis,[3] and Pengfei Wang[1,4,*]

[1]Key Laboratory of In-Fibre Integrated Optics of Ministry of Education, College of Science, Harbin Engineering University, Harbin 150001, China
[2]Photonics Research Centre, Technological University Dublin, Kevin Street, Dublin 8, Ireland
[3]Optical Fibre Sensors Research Centre, Department of Electronic and Computer Engineering, University of Limerick, Limerick V94 T9PX, Ireland
[4]Key Laboratory of Optoelectronic Devices and Systems of Ministry of Education and Guangdong Province, College of Optoelectronic Engineering, Shenzhen University, Shenzhen 518060, China
*Corresponding author: pengfei.wang@dit.ie

Received 12 March 2019; revised 17 March 2019; accepted 17 March 2019; posted 18 March 2019 (Doc. ID 362167); published 3 May 2019

A black phosphorus (BP) functionalized optical fiber sensor based on a microfiber coil resonator (MCR) for Pb^{2+} ion detection in an aquatic environment is presented and experimentally demonstrated. The MCR-BP sensor is manufactured by winding a tapered microfiber on a hollow rod composed of a low-refractive-index polycarbonate (PC) resin with the BP deposited on the internal wall of the rod. Based on the propagation properties of the MCR, the chemical interaction between the Pb^{2+} ions and the BP alters the refractive index of the ambient environment and thus results in a detectable shift in the transmission spectrum. The resonance wavelength moves towards longer wavelengths with an increasing concentration of Pb^{2+} ions, and the sensor has an ultra-high detection resolution of 0.0285 ppb (parts per billion). The temperature dependence is 106.95 pm/°C due to the strong thermo-optic and thermal-expansion effect of the low-refractive-index PC resin. In addition, the sensor shows good stability over a period of 15 days. The local pH also influences the sensor, with the resonance wavelength shift increasing as pH approaches a value of 7 but then decreasing as the pH value increases further due to the effect of the BP layer by H^+ and OH^- ions. The sensor shows the potential for high-resolution detection of Pb^{2+} ions in a liquid environment with the particular advantages of having a simple structure, ease of fabrication, low cost, low loss, and simple interrogation.

https://doi.org/10.1364/PRJ.7.000622

1. INTRODUCTION

In recent years, environmental water contamination has been a primary concern that needs to be addressed in the process of environmental protection. Among the possible forms of environmental pollution, toxic heavy metal pollution has become an enormous problem due to its destructive effect on the natural environment and human health [1,2]. Lead ions (Pb^{2+}) are a widespread contaminant that are highly toxic, do not degrade with time, and can be easily adsorbed, concentrated, and enriched by biological feeding, the ingestion of which can cause human health issues such as cardiovascular diseases, neurological disorders, brain damage, and mental deficiency [3–6]. Due to the growing presence of toxic lead compounds in agriculture and industry, the safety of aquatic environments is a major problem. According to the standards of the World Health Organization, the permissible limit of Pb^{2+} in potable water is 10 ppb (parts per billion) [7]. In order to monitor Pb^{2+} in aquatic environments, there are several methods such as inductively coupled plasma mass spectrometry [8], atomic absorption spectrometry [9], and fluorescence-based methods [10]. These methods can measure Pb^{2+} accurately, but the need for complex detection setups and expensive instrumentation impedes their application for practical detection and has limited their use in the laboratory.

Optical fiber sensors (OFSs) have become increasingly investigated as potential candidates for sensing because of their advantages of having low cost, light weight, and compact dimensions [11,12]. Many optical fiber sensors have already been applied in areas such as biosensing [13], gas sensing [14], temperature sensing [15], volatile compound sensing [16], and heavy metal detection [17]. Sensors based on microfibers have also been widely used as a result of their attractive characteristics including compact structure, small sensor volume and

weight, low loss, efficient evanescent field coupling, high quality factor, and high sensitivity. A number of variations have been demonstrated such as microfiber resonators [18], tapered microfibers [19], microfiber Bragg gratings [20], microfiber couplers [21], and microfiber based Fabry–Perot interferometers [22]. Microfiber resonators are sensitive to their ambient environment due to the very strong evanescent field interaction possible with the surrounding environment. Microfiber resonators can be split into three basic forms: loop [23], knot [24], and coil [25]. Microfiber coil resonators (MCRs) have the most sophisticated structure and are one of the few structures that are three-dimensional (3D). Although the 3D structure of MCRs may appear to have greater complexity, the benefit is that the coupling length is much longer due to the use of multiple turns within the coil, compared to microfiber loop and knot resonators, which have a comparatively short length for coupling. Furthermore, the relatively facile fabrication of the MCR described in this paper negates any disadvantage due to complexity. Hence MCRs have the potential for very high sensitivity and have been widely applied in temperature [26], refractive index [27], salinity [28], and electric current sensing [29]. There have also been many studies of heavy metal ion detection using methods based on optical fiber sensors, but to date and to the best of the knowledge of the authors of this paper, heavy metal ion sensing based on an MCR has not been reported in the literature.

Two-dimensional (2D) materials, including graphene [30], boron/carbon nitride [31], transition metal di-chalcogenides [32], and black phosphorus (BP) [33], have attracted significant recent research attention [34–36]. Based on their extraordinary attributes such as an atom-thin layer structure, a large surface-to-volume ratio, and high charge carrier mobility, 2D materials have seen wide application in electronics [32], energy storage [37], light processing [38], and chemical and biological sensors [39]. Recently, black phosphorus has also attracted attention in the wider areas of physics, chemistry, biology, and materials science [40–42]. BP has a layered structure, which has a pleated lattice structure along the armchair direction and a layer structure along a zigzag direction [43]. Due to its unique pleated construction and in-plane anisotropy, BP has quite large surface-to-volume ratio, extremely high hole mobility, and steerable light absorption compared to other 2D materials [44]. The particular properties of BP make it usable in a wide range of applications such as modulators [45], field-effect transistors [46], photodetectors [47], gas sensors [48], and photothermal therapy [49].

In this paper, an optical sensor for Pb^{2+} ion measurement in water using an MCR with a deposited layer of black phosphorus (BP) is described (BP-MCR). The BP-MCR sensor was fabricated by winding a tapered microfiber on a hollow rod formed from a low-refractive-index polycarbonate (PC) resin. Light propagation in the case of the MCR is very sensitive to the refractive index of its surrounding environment, and the interaction between the BP and heavy metal ions alters the refractive index through conjugation so that the sensor is sensitive to the concentration of heavy metal ions in a surrounding fluid. The resonance wavelength of the MCR moves towards long wavelengths as the Pb^{2+} concentration increases, and the sensor shows itself to be highly sensitive to Pb^{2+} with an ultra-high-resolution detection capability of 0.0285 ppb, which is better than the other methods formerly reported [50]. The temperature dependence of the sensor is as high as 106.95 pm/°C due to the strong thermo-optic and thermal-expansion effect from the low-refractive-index PC resin. In addition, the sensor has exhibited excellent stability while repeatedly recording over a 15-day period. The sensor was also tested in the presence of variation of pH of the liquid. If exposed to different pH solutions, the magnitude of the resonance wavelength shift increases in the range 1.3–7 at first but then decreases after the pH value exceeds 7 due to the influence of H^+ and OH^- ions for the combination between BP and Pb^{2+}. The sensor is therefore an excellent potential candidate to be used for ultra-high-resolution detection of a Pb^{2+} ion liquid environment and thus could be used in areas such as chemical sensing as well as detection in drinking water and waste water.

2. EXPERIMENTAL INSTALLATION AND PROCESSING

An optical-fiber-based MCR is generally a structure that is constituted by winding a tapered microfiber on a rod with lower refractive index (RI) than the microfiber. The MCR is shown in schematic diagram form in Fig. 1(a). The light propagation in the MCR has two paths: moving along the microfiber in a conventional manner but also moving in both the forward and backward directions through strong evanescent field coupling between adjacent turns. The light propagation in an MCR coil with n turns can be expressed as [51]

$$-i\frac{\mathrm{d}}{\mathrm{d}l}\begin{bmatrix} A_1(l) \\ A_2(l) \\ A_3(l) \\ \vdots \\ A_{n-2}(l) \\ A_{n-1}(l) \\ A_n(l) \end{bmatrix} = \begin{bmatrix} 0 & k & 0 & 0 & \cdots & 0 & 0 & 0 \\ k & 0 & k & 0 & \cdots & 0 & 0 & 0 \\ 0 & k & 0 & k & \cdots & 0 & 0 & 0 \\ \vdots & \vdots & \vdots & \vdots & & \vdots & \vdots & \vdots \\ 0 & 0 & 0 & 0 & \cdots & 0 & k & 0 \\ 0 & 0 & 0 & 0 & \cdots & k & 0 & k \\ 0 & 0 & 0 & 0 & \cdots & 0 & k & 0 \end{bmatrix} \begin{bmatrix} A_1(l) \\ A_2(l) \\ A_3(l) \\ \vdots \\ A_{n-2}(l) \\ A_{n-1}(l) \\ A_n(l) \end{bmatrix}, \tag{1}$$

where $A_i(l)$ is the electric field amplitude of the ith turn that varies along the turn over the turn length l and where k is the coupling coefficient between two adjacent coils. Given the continuous nature of the wound fiber, the output light amplitude of the ith coil must be equivalent to the input light amplitude of the $(i+1)$th coil, which implies the following continuity condition:

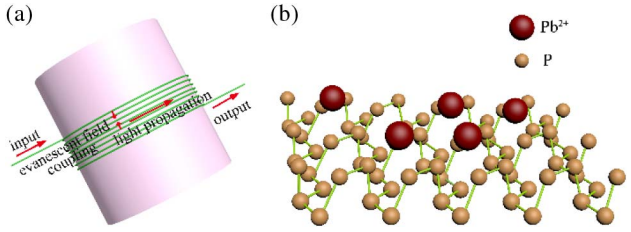

Fig. 1. (a) Schematic diagram of the MCR. (b) Adsorption between BP and Pb^{2+}.

$$\begin{bmatrix} A_1(0) \\ A_2(0) \\ A_3(0) \\ \vdots \\ A_{n-2}(0) \\ A_{n-1}(0) \\ A_n(0) \end{bmatrix} = \begin{bmatrix} 0 & 0 & 0 & \cdots & 0 & 0 & 0 \\ \exp^{i\beta l} & 0 & 0 & \cdots & 0 & 0 & 0 \\ 0 & \exp^{i\beta l} & 0 & \cdots & 0 & 0 & 0 \\ \vdots & \vdots & \vdots & & \vdots & \vdots & \vdots \\ 0 & 0 & 0 & \cdots & 0 & 0 & 0 \\ 0 & 0 & 0 & \cdots & \exp^{i\beta l} & 0 & 0 \\ 0 & 0 & 0 & \cdots & 0 & \exp^{i\beta l} & 0 \end{bmatrix} \times \begin{bmatrix} A_1(l) \\ A_2(l) \\ A_3(l) \\ \vdots \\ A_{n-2}(l) \\ A_{n-1}(l) \\ A_n(l) \end{bmatrix} + \begin{bmatrix} A_1(0) \\ 0 \\ 0 \\ \vdots \\ 0 \\ 0 \\ 0 \end{bmatrix}, \quad (2)$$

where β is the propagation constant of the fundamental mode (HE_{11}) and L is the length of each coil. β can be expressed by

$$\beta = \frac{2\pi n_{\text{eff}}}{\lambda}, \quad (3)$$

where n_{eff} is the effective index and λ is the wavelength.

The input of the MCR is defined as $A_1(0)$, while the output of the MCR is given by $A_n(L)\exp(i\beta L)$. The amplitude transmittance of the MCR is defined as

$$T = \frac{A_n(L)\exp(i\beta L)}{A_1(0)}. \quad (4)$$

From Eq. (1) to Eq. (4), assuming other conditions are kept constant, variations in the RI of the ambient environment will lead to variations in the propagation constant β in the MCR, and therefore the amplitude transmitted intensity of the light propagating in the MCR will change correspondingly, resulting in a detectable shift in transmission spectrum due to the relationship between amplitude transmitted intensity and transmission spectrum.

The Pb^{2+} ions are adsorbed by the BP due to van der Waals force and electrostatic interaction, as shown in Fig. 1(b). When the BP is in contact with the Pb^{2+}, Pb^{2+} forms a chelate compound on the surface of the BP. The mutual effect between BP and Pb^{2+} alters the RI of the conjugation, and in turn this results in shift in the transmission spectrum [52,53]. Therefore, a change in the concentration of Pb^{2+} in the solution can be detected by monitoring the variation of the transmission spectrum.

3. EXPERIMENT

The fabrication process for the BP-MCR sensor can be split into two distinct stages: (1) a fluidic channel is formed using a hollow rod onto which the MCR fiber is wound and secured in place and (2) BP nanosheets are adhered to the inner wall of the fluidic channel.

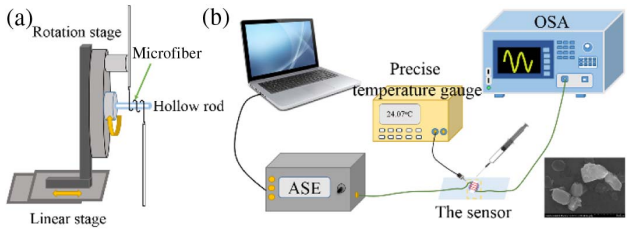

Fig. 2. (a) Schematic diagram of MCR fabrication process. (b) Schematic diagram of BP deposition and the Pb^{2+} detection process. The inset in (b) shows the scanning electron microscopy image of the BP nanosheets.

In more detail, in the first stage of the process a PMMA rod (Goodfellow, ME207901) with a length of 2 cm and diameter of 1 mm was packaged using a UV-curable low-refractive-index PC resin (Luvantix, PC373) and fully cured using a UV lamp (Lightningcure, LC8). The rod was then immersed in acetone for 6 h to dissolve the PMMA material, which resulted in a rod that is hollow and cylindrical and thus forms a simple fluidic channel. A tapered microfiber was then fabricated by stretching a standard single-mode fiber (Corning SMF 28) heated using a ceramic heat emitter [28]. The fabricated microfiber was wound around a PC resin tube with an inner diameter of 1 mm and a wall thickness of 0.18 mm to form a four-turn MCR with a central fluidic channel, as shown in Fig. 2(a). The device was then packaged using the same low-refractive-index PC resin and completely cured. For convenience, ease of measurement, and strong mechanical stability, the device was secured on a glass slide coated with the same low-refractive-index PC resin, which was once again cured using the same UV lamp.

In the second stage of the process, BP nanosheets were deposited on the inner wall of the fluidic channel formed above. The transmission spectrum of the BP-MCR sensor was monitored by an optical spectrum analyzer (OSA) (Yokogawa, AQ-6370C) in real time during the BP deposition process to determine if BP is deposited on the inner wall, and the ambient temperature was monitored by a precise temperature gauge (Burster, KELVIMAT4323) to guarantee that the experimental environment temperature is homogeneous. The input fiber of the sensor was irradiated using a broadband amplified spontaneous emission (ASE) source (YSL SC-series), and the output was measured using an OSA, as shown in Fig. 2(b). Using a syringe, a BP aqueous solution (XF 207, 7723-14-0, 102046) was injected into the fluidic channel, and the inset in Fig. 2(b) shows the complete lamellar structure of BP nanosheets. The water in the BP aqueous solution was allowed to fully evaporate so that the contact area between the UV-curable low-refractive-index PC resin rod wall was coated with BP nanosheets by photodeposition. Subsequently, further deposition cycles were conducted. In each cycle, the BP aqueous solution was injected into the fluidic channel, and the water was allowed to evaporate gradually and totally. After the fifth deposition cycle, the fabricated BP-MCR sensor was accomplished and prepared for use for Pb^{2+} ion detection.

4. RESULTS AND DISCUSSION

Initially, for reference purposes, a sensor without the BP deposition for sensing of Pb^{2+} was characterized. The sensor

without BP deposition was injected with $PbCl_2$ aqueous solutions with different concentrations from 0 to 13.9%. The experimental results are shown in Fig. 3. The transmission spectra were measured and recorded using the OSA. As shown in Fig. 3(a), as the Pb^{2+} concentration increases, the resonance wavelength moves towards a longer wavelength. The redshift is caused by the effective RI change of the MCR because of the change of the ambient RI, in turn caused by the different levels of Pb^{2+} concentration in the aqueous solution. For $PbCl_2$ concentrations from 0.1 to 50 ppb, the spectra are almost unchanged. In order to determine the influence from the effect of change in RI for different $PbCl_2$ concentrations, the transmission spectrum of a non-functionalized sensor without BP deposition was monitored for a large concentration range with about 1.8×10^6 ppb of $PbCl_2$ solution, and the RI was measured by an Abbe refractive index instrument. Figure 3(b) shows the dependence of resonance wavelength shift on the RI. It serves to show that the resonance wavelength shift of the non-functionalized sensor has a linear response to the RI of $PbCl_2$ solution, and the sensitivity is 4651.92 nm/RIU.

The transmission spectra of the sensor during one BP deposition process were recorded using the OSA. A BP aqueous solution was deposited slowly using the photodeposition technique as described above. A redshift resonance wavelength monitored during the deposition is shown in Fig. 4(a) and Fig. 4(b). It serves to show that following an elapsed time of about 30 min from the start of the experiment, the resonance wavelength change became negligible. This indicates that the process of the deposition of BP changes the effective RI of the fundamental mode in the MCR and thus the resonance wavelength, and it shows that the deposition of BP on the MCR stabilizes after about 30 min.

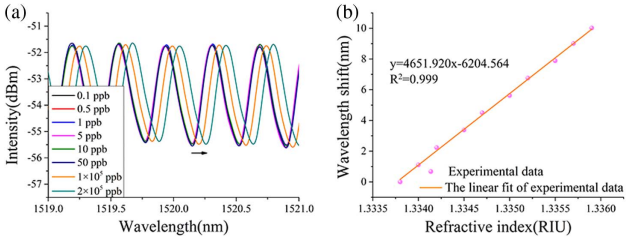

Fig. 3. (a) Spectral response of sensor without BP functionalized to varying Pb^{2+} concentration. (b) Sensitivity curve for refractive index for a non-functionalized sensor without BP deposition.

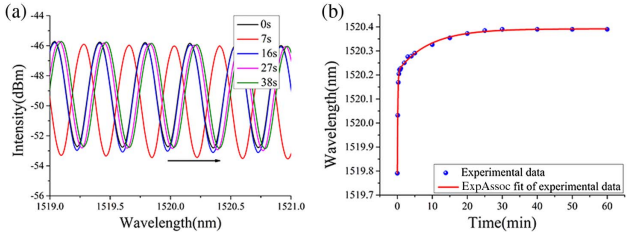

Fig. 4. (a) Transmission spectra in the BP deposition. (b) Response time curve for the deposition of BP on the MCR.

The optical characteristics of the BP-MCR sensor were investigated by measuring the transmission spectrum of the sensor with repeated BP deposition cycles, as shown in Fig. 5. The transmission spectrum was recorded using the OSA before application of any BP and following subsequent deposition cycles. It is apparent that the resonance wavelength has a redshift and the extinction ratio decreases as the thickness of the BP nanosheet layers increases, which was determined by the number of deposition cycles, as shown in Figs. 6(a) and 6(b). The redshift of the resonance wavelength can be ascribed to the change in effective RI caused by the high refractive index of BP. The MCR leaky radiation caused by the BP deposition could reduce the coupling between adjacent fibers and therefore decrease the extinction ratio.

A series of aqueous solutions of $PbCl_2$ were prepared for the detection and to determine the sensitivity of the sensor; the sensor that had undergone five BP nanosheet deposition cycles was chosen for the investigation. A reference spectrum of the sensor injected with deionized water (DI) was recorded before the spectra for Pb^{2+} aqueous solutions were recorded. The $PbCl_2$ solution was injected into the fluidic channel using a syringe, and the transmission spectrum was recorded using the OSA over the full duration of the immersion. Then the solution was sucked out 10 min after the spectrum was stable. The sensor was then thoroughly and repeatedly rinsed with deionized water. For different concentrations of Pb^{2+} solution,

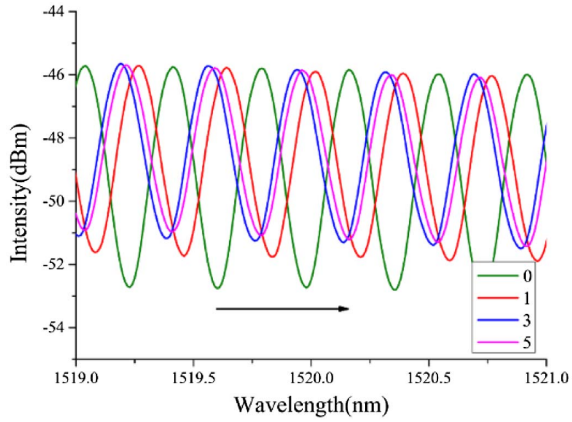

Fig. 5. Spectral evolution before and after several cycles of BP deposition.

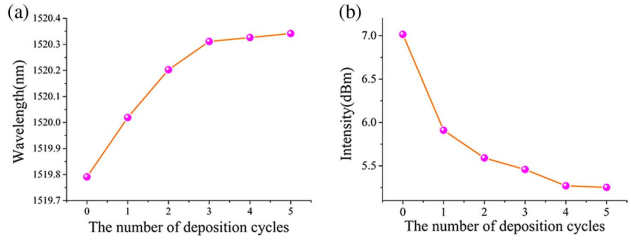

Fig. 6. (a) Resonance wavelength change against the number of deposition cycles. (b) Extinction ratio change against the number of deposition cycles.

the transmission spectra of the BP-MCR sensor are shown in Fig. 7(a). For an increasing Pb^{2+} concentration, a redshift of the resonance wavelength is observed as a result of the optical surface adsorption effect between the BP and Pb^{2+} ions: the Pb^{2+} ions are adsorbed by the BP due to the effect of van der Waals force and electrostatic interaction, as shown in Fig. 1(b). When the BP is in contact with the Pb^{2+}, Pb^{2+} forms a chelate compound on the surface of the BP. The mutual effect between BP and Pb^{2+} alters the refractive index of the conjugation, and in turn this results in the modulation (shift) of transmission spectrum. It serves to show that the resonance wavelength shift is apparent even at low concentrations of Pb^{2+} with 0 to 5×10^4 ppb.

Figure 7(b) shows the Pb^{2+} sensitivity contrast between a non-functionalized sensor and a BP functionalized sensor.

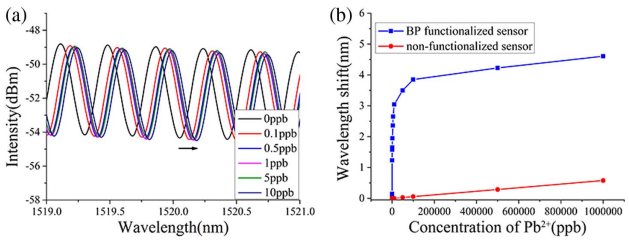

Fig. 7. (a) Transmission spectra of the BP-MCR sensor with different concentrations of Pb^{2+}. (b) Sensitivity comparison between non-functionalized and BP functionalized sensors.

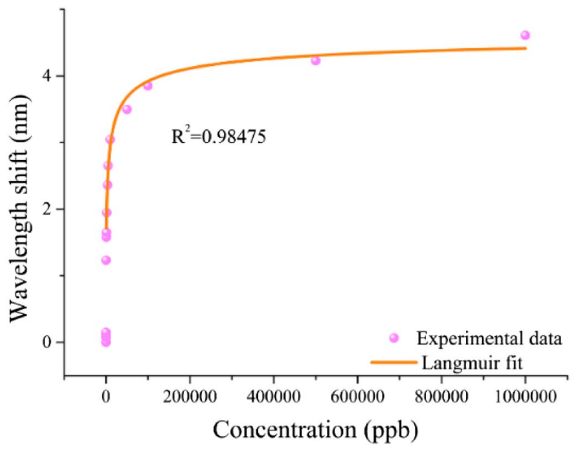

Fig. 8. Langmuir mode of the resonance wavelength shift with concentration of Pb^{2+}.

It serves to show that the sensor functionalized with BP has superior sensitivity compared to the non-functionalized sensor. In particular, the non-functionalized sensor shows a relatively low resonance wavelength shift when the Pb^{2+} concentration is low (less than 5×10^4 ppb), while for the BP functionalized sensor there is a much greater wavelength shift in the same low Pb^{2+} concentration range. The reason is that the effective RI of the environment close to the MCR is altered once the Pb^{2+} is bonded to the BP in the contact areas of the hollow rod and microfiber. For the non-functionalized sensor, there is no reaction between Pb^{2+} and the MCR. Therefore, the RI of the non-functionalized sensor shows almost no change with the concentration of Pb^{2+} in the low concentration range, and this change is only discernible when the Pb^{2+} concentration change is large (>400 ppm, parts per million).

Figure 8 shows the relationship between the resonance wavelength shift and the concentration of Pb^{2+} based on assuming the presence of a Langmuir adsorption mode [54]. The experimental result shows a good fit with the Langmuir mode ($R^2 = 0.98475$).

The lower limit of detection (LOD) is a key parameter when describing a sensor's characteristics, which can be defined as the lower concentration value that can be measured using the sensor. If the spectral resolution of the OSA is considered to be 0.02 nm (as specified by the manufacturer), the LOD of the BP-MCR sensor is 0.0285 ppb for Pb^{2+} ions as calculated on the basis of the Langmuir mode in Fig. 8. This is well below the World Health Organization (WHO) guide value and shows a 10-fold improvement over that of BP sensor based on an integrated tilted fiber grating [53]. To indicate the sensor performance over other sensors for Pb^{2+} detection, a summary of five different but comparable sensors is shown in Table 1. The LOD of the sensor of this investigation offers the best LOD, confirming a key advantage of the sensor described in this paper compared with sensors reported previously.

The response time of the BP-MCR sensor was also investigated. The response time is affected by the diffusion of Pb^{2+} to the BP interface and the rate of solid-phase adsorption of the metal by the BP. The response time of the sensor was measured for the Pb^{2+} solution with concentration values of 0.1, 10, and 100 ppb, as shown in Fig. 9. It serves to show that the sensor was found to reach 90% of the final wavelength shift in about 40–60 s, depending on the Pb^{2+} concentration, with a lower response time on higher concentration (about 56 s for 0.1 ppb, 51 s for 10 ppb, and 45 s for 100 ppb).

The temperature dependence of the BP-MCR sensor was also measured using an environmental chamber (ESPEC SH-222). Figure 10 shows the temperature dependence of

Table 1. Summary of Different Kinds of Sensors for Pb^{2+} Detection

No.	Modified Object	Materials	LOD (ppb)	Reference
1	Screen-printed carbon electrode	Graphene/polyaniline/polystyrene nanoporous fiber	3.3	[55]
2	Screen-printed carbon electrode	Bi nanoparticles	0.9	[56]
3	Glassy carbon electrode	Liquid phase-exfoliated graphene nanosheets	1.82	[57]
4	Chlorinated polyethylene	Bismuth nanoparticle-porous	0.65	[58]
5	U-shaped optical fiber probe	Oxalic acid functionalized Au nanoparticles	1.75	[50]
6	Microfiber coil resonator	Black phosphorus	0.0285	This work

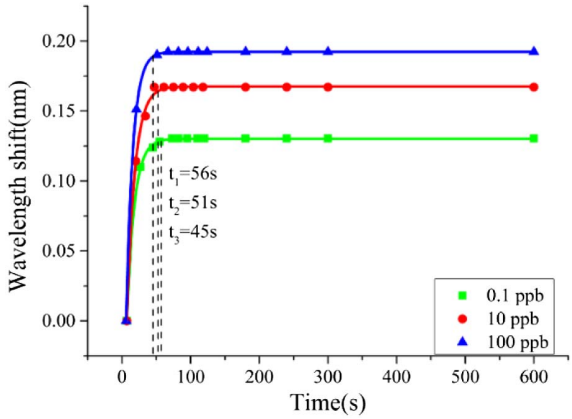

Fig. 9. Response time curves with the BP-MCR sensor immersed in Pb^{2+} concentrations of 0.1, 10, and 100 ppb.

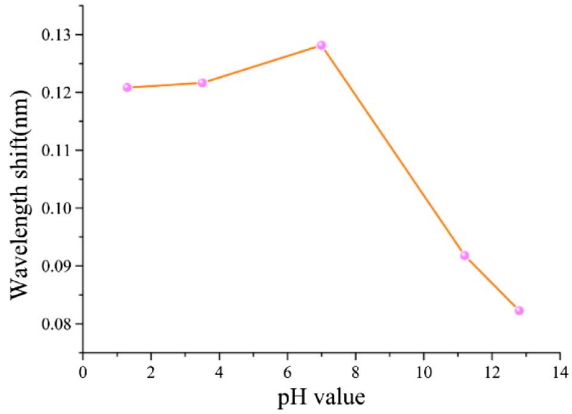

Fig. 11. Resonance wavelength shift of the BP-MCR sensor with different pH values of the solution.

the BP-MCR sensor. It can be seen that the resonance wavelength shifts towards longer wavelengths with increasing temperature, as shown in Fig. 10(a). The temperature sensitivity depends on four factors: the microfiber diameter, the diameter of the fluidic channel, the number of coils, and the gap between the adjacent coils [26]. It can also be seen that the sensor shows a linear relationship with temperature variations between 20°C and 25°C. As shown in Fig. 10(b), the temperature sensitivity is comparatively high with a value of 106.95 pm/°C due to the high thermal-expansion effect and thermo-optic effect from the low-refractive-index PC resin. The temperature sensitivity can be decreased by controlling the influence of the factors mentioned above and by changing to an alternative low refractive epoxy that has a lower thermal expansion coefficient and thermo-optic coefficient. Another method utilizes a combination of polymer and silica fiber Bragg gratings, which has a negative temperature sensitivity, and using a suitable interrogation scheme can counteract the high temperature dependence of the BP-MCR sensor [59].

The properties of the BP-MCR sensor can also be affected by the pH value of the solution [60]. As shown in Fig. 11, the pH dependence of the sensor for a 10 ppb Pb^{2+} concentration at various pH levels was investigated. The resonance wavelength shift increases within a narrow range at first but then decreases drastically with the pH value increasing from 1.3 to 12.8. In an acidic environment (pH < 7), H^+ ions compete with Pb^{2+} ions for combination to the BP, leading to a minor

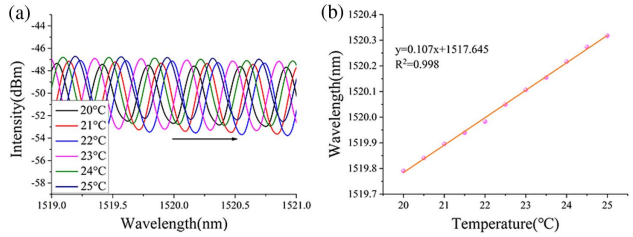

Fig. 10. (a) Transmission spectra of the BP functionalized sensor at different temperatures. (b) Linear fitting of the temperature response of the BP functionalized sensor. The points are experimental data, and the line is the linear fit of experimental data to temperature.

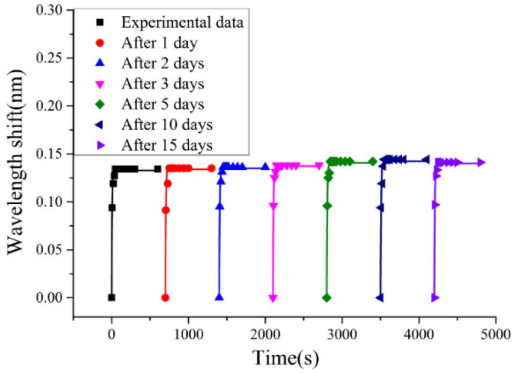

Fig. 12. Resonance wavelength shifts of the BP functionalized sensor for Pb^{2+} solutions after different durations.

wavelength shift as the concentration of the H^+ ions increases (pH decreasing below 7). When the pH level increases towards 7, the concentration of H^+ in the solution decreases, and thus the adsorption ability of the BP to Pb^{2+} is enhanced and then the resonance wavelength shift increases. Furthermore, as the pH level increases further above a pH value of 7 (alkaline environment), the OH^- ion concentration in the liquid increases and Pb^{2+} ions tend to form a precipitation, which gives rise to the decrease of Pb^{2+} concentration and the decrease of resonance wavelength shift.

Finally, the stability of the BP-MCR sensor was evaluated by taking measurements on the same Pb^{2+} solution with a concentration of 10 ppb repeatedly over a period of 15 days. The experimental results are shown in Fig. 12. It serves to show that the variation of the resonance wavelength shift is not significant in the results of multiple measurements, indicating the sensor has a good stability.

5. CONCLUSION

In this work, we have fabricated a BP functionalized optical fiber sensor based on an MCR for detection of Pb^{2+} ions in an aquatic environment. The BP-MCR sensor was manufactured by winding a tapered microfiber on a hollow rod composed of

a UV-curable low-refractive-index PC resin, and the BP was deposited on the inner wall of the rod. Based on the known propagation characteristics of the MCR, interaction of Pb^{2+} ions and BP resulted in changes of the refractive index of the liquid in the vicinity of the MCR, which in turn altered the transmission spectrum of the sensor. The measured resonance wavelength moved towards a longer wavelength with increasing Pb^{2+} ion concentration, and the results show that it is highly sensitive to Pb^{2+} concentration with an ultra-high detection resolution of 0.0285 ppb. The temperature dependence of the sensor of this investigation was up to 106.95 pm/°C, and this exists due to the strong thermo-optic and thermal-expansion effect from the UV-curable low-refractive-index PC resin. Extensive long-term testing showed that the sensor remains stable over a 15-day period. The resonance wavelength shift increases as the pH value increases at first, but then decreases after the value exceeds 7 due to the effect of H^+ and OH^- ions on the sensor surface. The sensor can uniquely be used in the low concentration range of Pb^{2+} ions with many valuable advantages, including a simple structure, ease of fabrication, low cost, low loss, and interrogation simplicity.

Funding. National Key R&D Program of China (2016YFE0126500); National Natural Science Foundation of China (NSFC) (61575050); Fundamental Research Funds for the Central Universities (HEUCFG201841); Key Program for Natural Science Foundation of Heilongjiang Province of China (ZD2016012); Open Fund of the State Key Laboratory on Integrated Optoelectronics (IOSKL2016KF03); 111 Project to the Harbin Engineering University (B13015).

REFERENCES

1. S. Thatai, P. Khurana, S. Prasad, S. K. Soni, and D. Kumar, "Trace colorimetric detection of Pb^{2+} using plasmonic gold nanoparticles and silica-gold nanocomposites," Microchem. J. **124**, 104–110 (2016).
2. K. Jomova and M. Morovič, "Effect of heavy metal treatment on molecular changes in root tips of *Lupinus luteus* L," Czech J. Food Sci. **27**, S386–S389 (2009).
3. B. Cheng, L. Zhou, L. Lu, J. Liu, X. Dong, F. Xi, and P. Chen, "Simultaneous label-free and pretreatment-free detection of heavy metal ions in complex samples using electrodes decorated with vertically ordered silica nanochannels," Sens. Actuators B **259**, 364–371 (2018).
4. H. Sun, L. Yu, H. Chen, J. Xiang, X. Zhang, Y. Shi, Q. Yang, A. Guan, Q. Li, and Y. Tang, "A colorimetric lead (II) ions sensor based on selective recognition of G-quadruplexes by a clip-like cyanine dye," Talanta **136**, 210–214 (2015).
5. Y. Lu, X. Li, G. Wang, and W. Tang, "A highly sensitive and selective optical sensor for Pb^{2+} by using conjugated polymers and label-free oligonucleotides," Biosens. Bioelectron. **39**, 231–235 (2013).
6. C. Hou, Y. Xiong, N. Fu, C. C. Jacquot, T. C. Squier, and H. Cao, "Turn-on ratiometric fluorescent sensor for Pb^{2+} detection," Tetrahedron Lett. **52**, 2692–2696 (2011).
7. R. Sedghi, S. Kazemi, and B. Heidari, "Novel selective and sensitive dual colorimetric sensor for mercury and lead ions derived from dithizone-polymeric nanocomposite hybrid," Sens. Actuators B **245**, 860–867 (2017).
8. P. T. Martinhon, J. Carreño, C. R. Sousa, O. E. Barcia, and O. R. Mattos, "Electrochemical impedance spectroscopy of lead (II) ion-selective solid-state membranes," Electrochim. Acta **51**, 3022–3028 (2006).
9. F. M. Pereira, D. M. Brum, F. G. Lepri, and R. J. Cassella, "Extraction induced by emulsion breaking as a tool for Ca and Mg determination in biodiesel by fast sequential flame atomic absorption spectrometry (FS-FAAS) using Co as internal standard," Microchem. J. **117**, 172–177 (2014).
10. A. Kumar, A. R. Chowdhuri, D. Laha, T. K. Mahto, P. Karmakar, and S. K. Sahu, "Green synthesis of carbon dots from *Ocimum sanctum* for effective fluorescent sensing of Pb^{2+} ions and live cell imaging," Sens. Actuators B **242**, 679–686 (2017).
11. P. Wang, G. Brambilla, M. Ding, Y. Semenova, Q. Wu, and G. Farrell, "High-sensitivity, evanescent field refractometric sensor based on a tapered, multimode fiber interference," Opt. Lett. **36**, 2233–2235 (2011).
12. A. Urrutia, J. Goicoechea, and F. J. Arregui, "Optical fiber sensors based on nanoparticle-embedded coatings," J. Sens. **2015**, 805053 (2015).
13. Y. Cao, X. Wang, T. Guo, Y. Ran, X. Feng, B.-O. Guan, and J. Yao, "High-resolution and temperature-compensational HER2 antigen detection based on microwave photonic interrogation," Sens. Actuators B **245**, 583–589 (2017).
14. S. P. Usha, S. K. Mishra, and B. D. Gupta, "Fabrication and characterization of a SPR based fiber optic sensor for the detection of chlorine gas using silver and zinc oxide," Materials **8**, 2204–2216 (2015).
15. Y. Wu, Y.-J. Rao, Y.-H. Chen, and Y. Gong, "Miniature fiber-optic temperature sensors based on silica/polymer microfiber knot resonators," Opt. Express **17**, 18142–18147 (2009).
16. S. Bagchi, R. Achla, and S. K. Mondal, "Electrospun polypyrrole-polyethylene oxide coated optical fiber sensor probe for detection of volatile compounds," Sens. Actuators B **250**, 52–60 (2017).
17. R. Raghunandhan, L. Chen, H. Long, L. Leam, P. So, X. Ning, and C. Chan, "Chitosan/PAA based fiber-optic interferometric sensor for heavy metal ions detection," Sens. Actuators B **233**, 31–38 (2016).
18. G. Brambilla, F. Xu, P. Horak, Y. Jung, F. Koizumi, N. P. Sessions, E. Koukharenko, X. Feng, G. S. Murugan, and J. S. Wilkinson, "Optical fiber nanowires and microwires: fabrication and applications," Adv. Opt. Photon. **1**, 107–161 (2009).
19. I. Hernández-Romano, D. Monzón-Hernández, C. Moreno-Hernández, D. Moreno-Hernandez, and J. Villatoro, "Highly sensitive temperature sensor based on a polymer-coated microfiber interferometer," IEEE Photon. Technol. Lett. **27**, 2591–2594 (2015).
20. B. Jiang, M. Xue, C. Zhao, D. Mao, K. Zhou, L. Zhang, and J. Zhao, "Refractometer probe based on a reflective carbon nanotube-modified microfiber Bragg grating," Appl. Opt. **55**, 7037–7041 (2016).
21. P. Wang, M. Ding, G. Brambilla, Y. Semenova, Q. Wu, and G. Farrell, "High temperature performance of an optical microfibre coupler and its potential use as a sensor," Electron. Lett. **48**, 283–284 (2012).
22. R. Wang and X. Qiao, "Intrinsic Fabry-Perot interferometeric sensor based on microfiber created by chemical etching," Sensors **14**, 16808–16815 (2014).
23. Y. Ren, R. Zhang, C. Ti, and Y. Liu, "Tapered optical fiber loops and helices for integrated photonic device characterization and microfluidic roller coasters," Optica **3**, 1205–1208 (2016).
24. Z. Xu, Q. Sun, B. Li, Y. Luo, W. Lu, D. Liu, P. P. Shum, and L. Zhang, "Highly sensitive refractive index sensor based on cascaded microfiber knots with Vernier effect," Opt. Express **23**, 6662–6672 (2015).
25. C.-J. Ma, L.-Y. Ren, Y.-P. Xu, Y.-L. Wang, H. Zhou, H.-W. Fu, and J. Wen, "Theoretical and experimental study of structural slow light in a microfiber coil resonator," Appl. Opt. **54**, 5619–5623 (2015).
26. Y. Yin, J. Yu, Y. Jiang, S. Li, J. Ren, G. Farrell, E. Lewis, and P. Wang, "Investigation of temperature dependence of microfiber coil resonators," J. Lightwave Technol. **36**, 4887–4893 (2018).
27. F. Xu and G. Brambilla, "Demonstration of a refractometric sensor based on optical microfiber coil resonator," Appl. Phys. Lett. **92**, 101126 (2008).
28. Y. Yin, S. Li, J. Ren, G. Farrell, E. Lewis, and P. Wang, "High-sensitivity salinity sensor based on optical microfiber coil resonator," Opt. Express **26**, 34633–34640 (2018).
29. S.-C. Yan, B.-C. Zheng, J.-H. Chen, F. Xu, and Y.-Q. Lu, "Optical electrical current sensor utilizing a graphene-microfiber-integrated coil resonator," Appl. Phys. Lett. **107**, 053502 (2015).
30. A. K. Geim, "Graphene: status and prospects," Science **324**, 1530–1534 (2009).

31. W. Lei, D. Portehault, R. Dimova, and M. Antonietti, "Boron carbon nitride nanostructures from salt melts: tunable water-soluble phosphors," J. Am. Chem. Soc. **133**, 7121–7127 (2011).
32. Q. H. Wang, K. Kalantar-Zadeh, A. Kis, J. N. Coleman, and M. S. Strano, "Electronics and optoelectronics of two-dimensional transition metal dichalcogenides," Nat. Nanotechnol. **7**, 699–712 (2012).
33. F. Xia, H. Wang, and Y. Jia, "Rediscovering black phosphorus as an anisotropic layered material for optoelectronics and electronics," Nat. Commun. **5**, 4458 (2014).
34. Y. Wang, F. Zhang, X. Tang, X. Chen, Y. Chen, W. Huang, Z. Liang, L. Wu, Y. Ge, and Y. Song, "All-optical phosphorene phase modulator with enhanced stability under ambient conditions," Laser Photon. Rev. **12**, 1800016 (2018).
35. Z. Guo, S. Chen, Z. Wang, Z. Yang, F. Liu, Y. Xu, J. Wang, Y. Yi, H. Zhang, and L. Liao, "Metal-ion-modified black phosphorus with enhanced stability and transistor performance," Adv. Mater. **29**, 1703811 (2017).
36. N. Michael, K. Murat, P. Volker, L. Jun, N. Junjie, H. Min, H. Lars, G. Yury, and M. W. Barsoum, "Two-dimensional nanocrystals produced by exfoliation of Ti_3AlC_2," Adv. Mater. **23**, 4248–4253 (2011).
37. Z.-S. Wu, G. Zhou, L.-C. Yin, W. Ren, F. Li, and H.-M. Cheng, "Graphene/metal oxide composite electrode materials for energy storage," Nano Energy **1**, 107–131 (2012).
38. Q. Bao, H. Zhang, Y. Wang, Z. Ni, Y. Yan, Z. X. Shen, K. P. Loh, and D. Y. Tang, "Atomic-layer graphene as a saturable absorber for ultrafast pulsed lasers," Adv. Funct. Mater. **19**, 3077–3083 (2009).
39. J. D. Fowler, M. J. Allen, V. C. Tung, Y. Yang, R. B. Kaner, and B. H. Weiller, "Practical chemical sensors from chemically derived graphene," ACS Nano **3**, 301–306 (2009).
40. L. Li, Y. Yu, G. J. Ye, Q. Ge, X. Ou, H. Wu, D. Feng, X. H. Chen, and Y. Zhang, "Black phosphorus field-effect transistors," Nat. Nanotechnol. **9**, 372–377 (2014).
41. S. C. Dhanabalan, J. S. Ponraj, Z. Guo, S. Li, Q. Bao, and H. Zhang, "Emerging trends in phosphorene fabrication towards next generation devices," Adv. Sci. **4**, 1600305 (2017).
42. M. Qiu, W. X. Ren, T. Jeong, M. Won, G. Y. Park, D. K. Sang, L.-P. Liu, H. Zhang, and J. S. Kim, "Omnipotent phosphorene: a next-generation, two-dimensional nanoplatform for multidisciplinary biomedical applications," Chem. Soc. Rev. **47**, 5588–5601 (2018).
43. A. Castellanos-Gomez, "Black phosphorus: narrow gap, wide applications," J. Phys. Chem. Lett. **6**, 4280–4291 (2015).
44. S. Y. Cho, Y. Lee, H. J. Koh, H. Jung, J. S. Kim, H. W. Yoo, J. Kim, and H. T. Jung, "Superior chemical sensing performance of black phosphorus: comparison with MoS_2 and graphene," Adv. Mater. **28**, 7020–7028 (2016).
45. R. Zhang, Y. Zhang, H. Yu, H. Zhang, R. Yang, B. Yang, Z. Liu, and J. Wang, "Broadband black phosphorus optical modulator in the spectral range from visible to mid-infrared," Adv. Opt. Mater. **3**, 1787–1792 (2015).
46. M. Buscema, D. J. Groenendijk, S. I. Blanter, G. A. Steele, H. S. Van Der Zant, and A. Castellanos-Gomez, "Fast and broadband photoresponse of few-layer black phosphorus field-effect transistors," Nano Lett. **14**, 3347–3352 (2014).
47. N. Youngblood, C. Chen, S. J. Koester, and M. Li, "Waveguide-integrated black phosphorus photodetector with high responsivity and low dark current," Nat. Photonics **9**, 247–252 (2015).
48. A. N. Abbas, B. Liu, L. Chen, Y. Ma, S. Cong, N. Aroonyadet, M. Köpf, T. Nilges, and C. Zhou, "Black phosphorus gas sensors," ACS Nano **9**, 5618–5624 (2015).
49. J. Shao, H. Xie, H. Huang, Z. Li, Z. Sun, Y. Xu, Q. Xiao, X.-F. Yu, Y. Zhao, and H. Zhang, "Biodegradable black phosphorus-based nanospheres for *in vivo* photothermal cancer therapy," Nat. Commun. **7**, 12967 (2016).
50. B. S. Boruah and R. Biswas, "Localized surface plasmon resonance based U-shaped optical fiber probe for the detection of Pb^{2+} in aqueous medium," Sens. Actuators B **276**, 89–94 (2018).
51. M. Sumetsky, "Optical fiber microcoil resonator," Opt. Express **12**, 2303–2316 (2004).
52. J. Kim, S. S. Baik, S. H. Ryu, Y. Sohn, S. Park, B.-G. Park, J. Denlinger, Y. Yi, H. J. Choi, and K. S. Kim, "Observation of tunable band gap and anisotropic Dirac semimetal state in black phosphorus," Science **349**, 723–726 (2015).
53. C. Liu, Z. Sun, L. Zhang, J. Lv, X. Yu, and X. Chen, "Black phosphorus integrated tilted fiber grating for ultrasensitive heavy metal sensing," Sens. Actuators B **257**, 1093–1098 (2018).
54. Y.-C. Chang and D.-H. Chen, "Preparation and adsorption properties of monodisperse chitosan-bound Fe_3O_4 magnetic nanoparticles for removal of Cu (II) ions," J. Colloid Interface Sci. **283**, 446–451 (2005).
55. N. Promphet, P. Rattanarat, R. Rangkupan, O. Chailapakul, and N. Rodthongkum, "An electrochemical sensor based on graphene/polyaniline/polystyrene nanoporous fibers modified electrode for simultaneous determination of lead and cadmium," Sens. Actuators B **207**, 526–534 (2015).
56. M. Á. G. Rico, M. Olivares-Marín, and E. P. Gil, "Modification of carbon screen-printed electrodes by adsorption of chemically synthesized Bi nanoparticles for the voltammetric stripping detection of Zn (II), Cd (II) and Pb (II)," Talanta **80**, 631–635 (2009).
57. G. Liu, J. Chen, X. Hou, and W. Huang, "A highly-sensitive electrochemical sensor for the simultaneous detection of Cd^{2+} and Pb^{2+} using liquid phase-exfoliated graphene," Anal. Methods **6**, 5760–5765 (2014).
58. P. Niu, C. Fernández-Sánchez, M. Gich, C. Ayora, and A. Roig, "Electroanalytical assessment of heavy metals in waters with bismuth nanoparticle-porous carbon paste electrodes," Electrochim. Acta **165**, 155–161 (2015).
59. H. Liu, H. Liu, G. Peng, and P. Chu, "Strain and temperature sensor using a combination of polymer and silica fibre Bragg gratings," Opt. Commun. **219**, 139–142 (2003).
60. Y.-N. Zhang, L. Zhang, B. Han, P. Gao, Q. Wu, and A. Zhang, "Reflective mercury ion and temperature sensor based on a functionalized no-core fiber combined with a fiber Bragg grating," Sens. Actuators B **272**, 331–339 (2018).